Misfit dislocation networks in the γ/γ' phase interface of a Ni-based single-crystal superalloy: Molecular dynamics simulations

Tao Zhu[1] and Chong-yu Wang[2,1,3]

[1]*Central Iron and Steel Research Institute, Beijing 100081, China*
[2]*China Center of Advanced Science and Technology (World Laboratory), P.O. Box 8730, Beijing 100080, China*
[3]*Department of Physics, Tsinghua University, Beijing 100084, China*

The structure of the γ/γ' phase interface in a Ni-based single-crystal superalloy is simulated by molecular dynamics (MD) using an embedded atom method potential. From the calculated results we find that three dislocation network patterns, namely square, rectangle, and equilateral triangle, appear on {100}, {110}, and {111} interphase interface, respectively. The dislocation networks consist of four edge dislocations ($\langle 011 \rangle$ {100}, $\langle \bar{1}10 \rangle$ {110}, $\langle 001 \rangle$ {110}, and $\langle 112 \rangle$ {111}). The energy of the γ/γ' phase interface for {100}, {110}, and {111} plane is 271 mJ/m², 240 mJ/m², and 32 mJ/m². The side length of network is 166.8 Å for the square, 166.8 Å and 235.8 Å for the rectangle and 166.8 Å for the equilateral triangle. The relationship between the size of network and mismatch is presented quantitatively. The calculated results can be supported by very recent experiments. Based on the MD simulation and the energy analysis we have revealed the basic characteristic of structure on γ/γ' phase interface. The related mechanism of the stability of the interphase interface is also discussed.

PACS number(s): 61.50.Ah, 61.72.Bb, 62.20.Fe, 68.35.Fx

I. INTRODUCTION

Nickel-based single-crystal superalloy is one of the most important structural materials for advanced aircraft turbine blade. It consists of a Ni-based matrix (fcc γ phase) with a dispersion strengthening phase, i.e., the ordered intermetallic precipitate particles of Ni₃Al (L1₂ γ' phase). In the single crystal superalloy, the γ' volume fraction can reach 70% or even higher. The particle size of about 0.45 μm appears to be optimum for the yield strength and creep strength and also for hot hardness.[1–3]

Both Ni and Ni₃Al possess face-centered-cubic structures, with very similar lattice parameters. The lattice parameter is 3.52 Å for fcc Ni (as a modeling γ phase in this work) and 3.567 Å (expt) or 3.573 Å (calc) for L1₂ Ni₃Al (as a modeling γ' phase in this work).[4] Because the lattice parameters of the two phases are not identical, the stress field resulting from the lattice mismatch will be created, which depends on the surface state of the precipitate phase. Obviously, the interphase interface with the stress field is unstable. Based on the principle of minimum energy, the atoms on the interphase interface will rearrange in order to minimize the elastic stress field between γ phase and γ' phase, i.e., a self-accommodating process. Then the network of the interphase interface dislocations will be created and the interphase coherence will be affected. This process shows that the formation of dislocation networks is an important way to reduce the distorted energy. From the above discussion it can be supposed that the interphase interfaces with dislocation networks will widely exist in the single-crystal superalloy, and will have great influence on the mechanical properties of the superalloy.

In the present work, the molecular dynamics (MD) method is used to simulate the γ/γ' phase interface with the indices of {100}, {110}, and {111} in the Ni-based single-

crystal superalloy. Regarding the crystallographic properties introduced by lattice misfit, we have proposed six initial models. Simulations are performed using Voter-Chen-type embedded atom method potential.[4] The results show that three different edge dislocation networks are formed on the interphase interface by the MD simulations. The related phenomena have been observed in recent experiments.[5–11] In this paper we focus on studying the characters of atomic configurations on the γ/γ' phase interface and exploring the related mechanism to understand the mechanical properties of the single-crystal superalloy.

II. MODELING AND SIMULATION

In this paper, the structure of the γ/γ' phase interface in the Ni-based single-crystal superalloy is simulated with molecular dynamics. The Voter-Chen-type (VC) embedded atom method (EAM) potential is used, which is very successful in the study on the Ni-Al system.[12–16]

As we know, the lattice misfit corresponds to the deformation of invariant lattice, and the mismatch δ is defined as the normalized difference in the lattice parameter between γ and γ', given by

$$\delta = 2\frac{a_{\gamma'} - a_\gamma}{a_{\gamma'} + a_\gamma}, \tag{1}$$

where a_γ is 3.52 Å, $a_{\gamma'}$ is 3.573 Å (calc); for the γ/γ' phase system, δ is 1.5% (calc).

When the mismatch exceeds the limit of elasticity, the misfit dislocation will be formed on the interphase interface to reduce the distorted energy of the system.[17] Considering the concept of coincidence site lattice (CSL) on the misfit interphase interface, we can write such a relation of
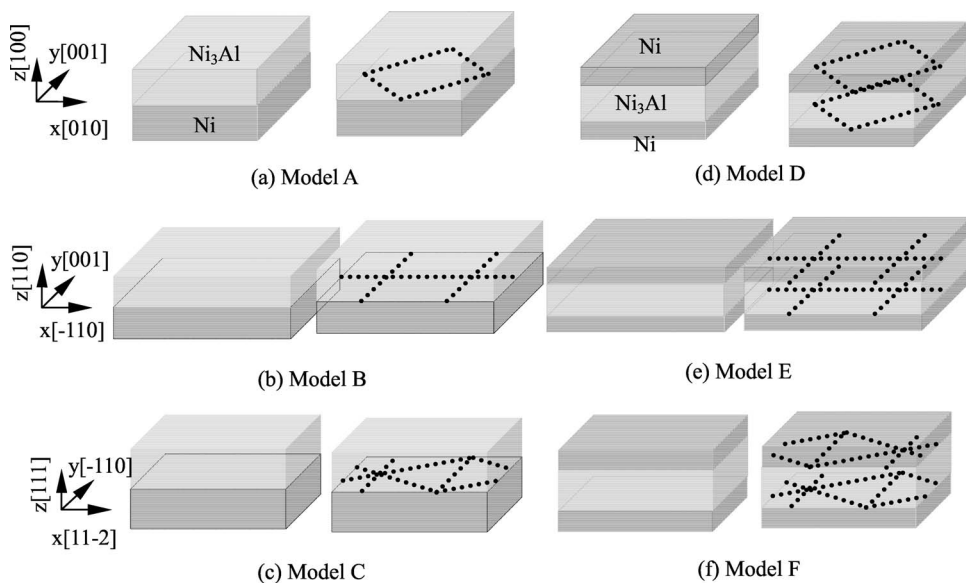
FIG. 1. The diagrammatic sketch of the initial models and the relaxation results. In models A, B, and C, periodic boundary conditions are employed in the x, y directions, free boundary condition is in the z direction. In models D, E, and F, the periodic boundary conditions are employed along all three directions. The misfit dislocation networks are formed on the interphase interface after relaxation.

$$na_{\gamma'} = (n+1)a_{\gamma}, \qquad (2)$$

where n is n-fold of the lattice parameter, for the γ / γ' phase system,

$$n = \frac{a_{\gamma}}{a_{\gamma'} - a_{\gamma}} \approx 66. \qquad (3)$$

It indicates that within the range of misfit interphase interface formed by 66 γ' lattices and 67 γ lattices, the stress induced by the difference of lattice parameters should be relaxed.

According to the above relaxed configuration we can construct different structure units of interphase interface. The created models are shown in Fig. 1. In the models A, B, and C, the periodic boundary conditions are employed along the

directions parallel to the interphase interface, while the free boundary condition is employed along the direction vertical to the interphase interface. Considering the γ' phase is a three-dimensional precipitate phase, we construct three "sandwich style" initial models D, E, and F. In these models, the γ' phase structure units are sandwiched in the γ phase structure units, so the periodic boundary conditions can be used along all three directions.

For the sake of comparison, the same amount of atoms are chosen in the six models. Moreover, in order to eliminate the effect of interactions between the interfaces, we choose a larger thickness to create our models, the thickness of the phase structure unit is $48a$ for models A and D, $24\sqrt{2}a$ for models B and E, and $8\sqrt{3}a$ for models C and F (see Table I).

Through the MD relaxation at $T=0$ K we can find the equilibrium atomic structure of dislocation on the γ / γ'

TABLE I. Atomic configurations of the initial models. Models A, B, and C are the structure units with one γ' block and one γ block. Models D, E, and F are the "sandwich style" structure units with one γ' block and two identical γ blocks. All the models with different interphase interfaces have 1489152 Ni atoms and 209088 Al atoms.

Model	Number of atoms in γ block (Ni-based fcc)	Number of atoms in γ' block (Ni$_3$Al L1$_2$)	Interphase interfaces and orientations (x, y, z)
A	Ni: $67 \times 67 \times 48 \times 4 = 861888$[a]	Ni: $66 \times 66 \times 48 \times 3 = 627264$	(100)
D	Ni: $67 \times 67 \times 24 \times 4 = 430944$	Al: $66 \times 66 \times 48 \times 1 = 209088$	$[010] [001] [100]$
	Ni: $67 \times 67 \times 24 \times 4 = 430944$		
B	Ni: $67\sqrt{2} \times 67 \times 24\sqrt{2} \times 4 = 861888$	Ni: $66\sqrt{2} \times 66 \times 24\sqrt{2} \times 3 = 627264$	(110)
E	Ni: $67\sqrt{2} \times 67 \times 12\sqrt{2} \times 4 = 430944$	Al: $66\sqrt{2} \times 66 \times 24\sqrt{2} \times 1 = 209088$	$[\bar{1}10] [001] [110]$
	Ni: $67\sqrt{2} \times 67 \times 12\sqrt{2} \times 4 = 430944$		
C	Ni: $67\sqrt{6} \times 67\sqrt{2} \times 8\sqrt{3} \times 4 = 861888$	Ni: $66\sqrt{6} \times 66\sqrt{2} \times 8\sqrt{3} \times 3 = 627264$	(111)
F	Ni: $67\sqrt{6} \times 67\sqrt{2} \times 4\sqrt{3} \times 4 = 430944$	Al: $66\sqrt{6} \times 66\sqrt{2} \times 8\sqrt{3} \times 1 = 209088$	$[11\bar{2}] [\bar{1}10] [111]$
	Ni: $67\sqrt{6} \times 67\sqrt{2} \times 4\sqrt{3} \times 4 = 430944$		

[a]$l_x \times l_y \times l_z \times n_a = N$, where l_x, l_y, and l_z are the size (in lattice parameter) of the structure units, n_a is the corresponding number of atoms in a primitive cell, and N is the number of atoms in the block.
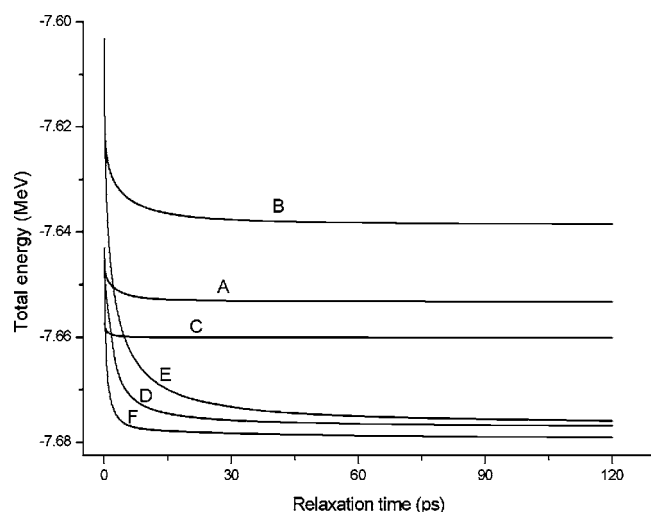
FIG. 2. Total energy (in MeV) as a function of the relaxation time (in ps) in the six models.

phase interface, which will be used in the first principle calculation to study the electronic structure and doping effect (we are undergoing). According to the tendency of convergence, the time steps taken are 6 fs (1 fs$=10^{-15}$ s) for models A and D, 3 fs for models B and E, and 8 fs for models C and F.

III. RESULTS AND DISCUSSION

The function of the total energy versus relaxation time is shown in Fig. 2. It reveals that with the same boundary conditions, the models B or E with {110} interphase interface reaches the equilibrium state by the slowest speed. After 100 ps (1 ps$=10^{-12}$ s) relaxation the biggest rate of change ($\Delta E_{\text{total}}/\Delta t_{\text{relaxation}}$) in the six models is only 6.12 eV/ps (for model E), which means that the systems have reached the equilibrium state. In this paper, models A, B, and C are used for the geometric and general qualitative analysis. For models D, E, and F, because the periodic boundary conditions are applied along all three directions and have no free surface, they will approach three-dimensional bulk. Therefore, all the energetic calculations can be performed on the basis of the simulation results of them.

Comparing the total energies at equilibrium states for models D, E, and F, we can see that for the {111} interphase interface the total energy is the lowest, the second is for the {100} interphase interface, and for the {110} interphase interface the energy is the highest. The results are consistent with that in fcc or for the L1$_2$ structures the {111} plane is the closest-packed plane, and the {100} plane is next to it.

To study the stability of interphase interface, we calculate the interphase interface energy between the γ and γ' phases for the models D, E, and F according to the following equation:

$$E_{\gamma/\gamma'} = \frac{E_{\text{sandwich}} - (E_{\gamma} + E_{\gamma'})}{2S}, \qquad (4)$$

where E_{sandwich} is the total energy of the sandwich model which contains two interphase interfaces, E_{γ} is the total en-

TABLE II. The γ/γ' phase interface energy (in mJ/m^2) for the different interphase interfaces.

Interphase interface	$E_{\gamma/\gamma'}$
(100)	271
(110)	240
(111)	32

ergy of the perfect γ matrix, $E_{\gamma'}$ is the total energy of the perfect γ' precipitates, and S is the surface area of the interphase interface. The results are listed in Table II.

From Table II, it is found that the interface energy $E_{\gamma/\gamma'}$ of {111} interphase interface is much lower than that of the other two, which means that $\langle 111 \rangle$ is the most favorable direction for the precipitation of γ' phase to grow.

In addition, we calculate the surface energies of Ni, Al, and Ni$_3$Al, which also present the stability of interphase interface in the precipitating process. Table III lists the calculated results and the experiment values[18] as well as the other's calculations.[14] The surface energy is given by

$$E_s = \frac{E_1 - E_2}{2S}, \qquad (5)$$

where E_1 is the total energy of a perfect lattice with surface (periodic boundary in two directions parallel to the interface, free surface in the other), E_2 is the total energy of a perfect lattice without surface (periodic boundaries in all three directions), and S is the surface area of the interface.

From Table III it can be found that the surface energies of Ni and Al are both in good agreement with the experiment results and other calculations.

Based on the potential energy of atoms, we have selected the atoms with the higher potential energies in the dislocation core area and along dislocation line. The patterns of the misfit dislocation networks in the six models are shown in Fig. 3. It can be seen that the misfit dislocation networks are

TABLE III. Surface energies (in mJ/m^2) in comparison with experimental and other work. The {111} surfaces have the lowest surface energies.

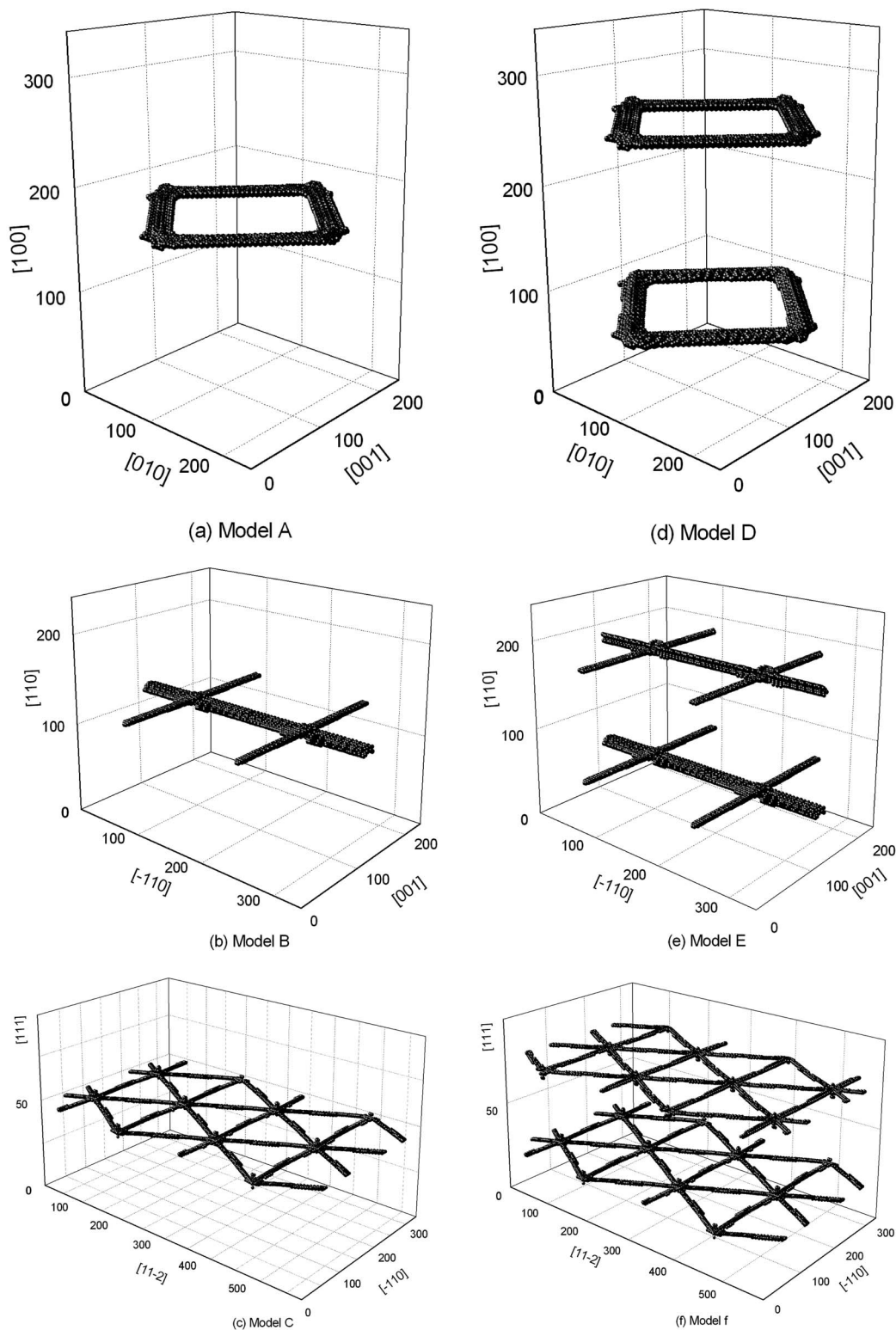| Object	Interphase interface	Present work	Mishin and Farkas (Ref. 14)	Expt. (Ref. 18)
Ni	(100)	1762	1878	
	(110)	2003	2049	2280±350
	(111)	1630	1629	
Al	(100)	869	943	
	(110)	1006	1006	980±150
	(111)	832	870	
Ni$_3$Al	(100)	1923		
	(110)	2081		
	(111)	1769		

FIG. 3. The patterns of the misfit dislocation networks in six models. The square, rectangle, and equilateral triangle networks are presented in the (100) interphase interface of (a) model A and (d) model D, (110) interphase interface of (b) model B and (e) model E, as well as (111) interphase interface of (c) model C and (f) model F, respectively. The side length of the networks is 166.8 Å for the square, 166.8 Å and 235.8 Å for the rectangle, and 166.8 Å for the equilateral triangle. The scales are given in Å.

formed in all the models, and the shape of each network only depends on the type of interphase interface. The square, rectangle, and equilateral triangle networks appear in {100}, {110}, and {111} interphase interface, respectively, and the side length of the networks is 166.8 Å for the square, 166.8 Å and 235.8 Å for the rectangle, and 166.8 Å for the
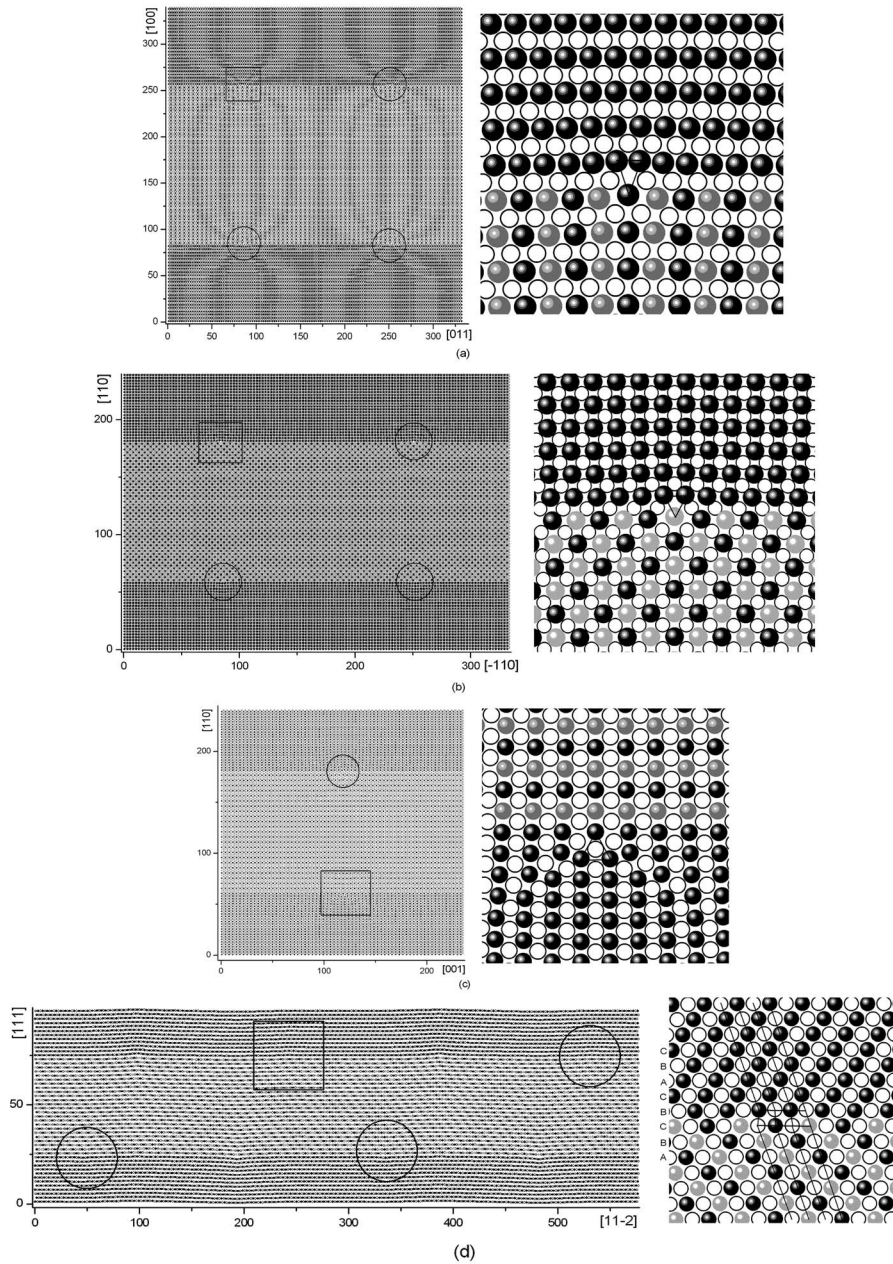
FIG. 4. The misfit dislocations on the interphase interface. The positions of dislocations are circled and the details are shown in (a) [the $[011]$ (100) edge dislocation], (b) [the $[\bar{1}10]$ (110) edge dislocation], (c) [the $[001]$ (110) edge dislocation], and (d) [the $[11\bar{2}]$ (111) edge dislocation], respectively. The spheres and circles represent different layers, and the grey spheres represent Al atoms. The scales are given in Å.

equilateral triangle. The simulation results indicate that the densest dislocations appear on the {111} interphase interface. Similar patterns have been observed in experiments with high resolution electron microscopy (HREM).[6–11]

From Fig. 3 and the calculated results, it can be seen that the size of the misfit dislocation network for the interphase interface is determined by the lattice parameters of γ phase and γ' phase. Based on the interphase interface models and the patterns of the dislocation networks, the side length d can be given as

$$d \propto \frac{a_\gamma a_{\gamma'}}{a_{\gamma'} - a_\gamma}, \tag{6}$$

where a_γ and $a_{\gamma'}$ are the lattice parameters of the γ phase and γ' phase, respectively. Considering Eq. (1), we find that

the dimension of the misfit dislocation network is correlated with the mismatch parameter of δ. Equation (6) then becomes

$$d \propto \left(\frac{1}{\delta} + \frac{1}{2}\right)a_\gamma \approx \frac{a_\gamma}{\delta}. \tag{7}$$

Equation (7) indicates that the larger the δ is, the smaller the d is. The relationship between δ and d can essentially explain the experimental observation referred to in the work of the National Institute for Materials Science (NIMS) in 2004.[9,10]

In order to determine the crystallographic indices of the dislocations, the atoms in the plane perpendicular to the dislocation line are drawn in Fig. 4. The results show that the three different dislocation networks are composed of four edge dislocations with indices of $\langle 011 \rangle$ {100}, $\langle \bar{1}10 \rangle$ {110},

TABLE IV. The edge dislocations correspond to the networks of the different interphase interfaces.

Interphase interface	Edge dislocation	Index
(100)	$[011](100)$	$\langle 011 \rangle \{100\}$
	$[0\bar{1}1](100)$	
(110)	$[\bar{1}10](110)$	$\langle \bar{1}10 \rangle \{110\}$
	$[001](110)$	$\langle 001 \rangle \{110\}$
(111)	$[11\bar{2}](111)$	
	$[1\bar{2}1](111)$	$\langle 112 \rangle \{111\}$
	$[\bar{2}11](111)$	

$\langle 001 \rangle \{110\}$, and $\langle 112 \rangle \{111\}$, where the slip plane is along the interface. In fact, in the (100) interface, the $[011]$ (100) and $[0\bar{1}1]$ (100) edge dislocations are equivalent, while in the (111) interface, the three edge dislocations $[11\bar{2}]$ (111), $[1\bar{2}1]$ (111), and $[\bar{2}11]$ (111) are equivalent. Table IV presents the relationships among the dislocation networks, interphase interface, and edge dislocation.

The above simulation results reveal that the distribution and characters of the dislocations are determined by the orientation and the mismatch parameter δ of γ/γ' phase interface. So it can be concluded that the formation of the dislocation networks will sensitively affect the deformation behavior, which is closely related to the mechanical properties of the materials.

IV. SUMMARY

By constructing the different models of interphase interface, we find that the misfit dislocation networks will be formed on the misfit interface after relaxation. Moreover, different shapes of network appear on the corresponding interphase interface, square on the $\{100\}$ interphase interface, rectangle on the $\{110\}$ interphase interface, and equilateral triangle on the $\{111\}$ interphase interface. The interphase interface energy of $\{100\}$, $\{110\}$, and $\{111\}$ plane is 271 mJ/m^2, 240 mJ/m^2, and 32 mJ/m^2, respectively. The side length of network is 166.8 Å for the square, 166.8 Å and 235.8 Å for the rectangle, and 166.8 Å for the equilateral triangle. Three different dislocation networks correspond to four edge dislocations with indices of $\langle 011 \rangle \{100\}$, $\langle \bar{1}10 \rangle \{110\}$, $\langle 001 \rangle \{110\}$, and $\langle 112 \rangle \{111\}$, where the slip plane is along the interphase interface. The simulation results indicate that the densest dislocations appear on the $\{111\}$ interphase interface. From the calculated interface energy and the surface energy we can predict that $\langle 111 \rangle$ is the most favorable direction for the precipitation of γ' phase to grow.

The dislocation networks determined by the orientation and the mismatch δ of γ/γ' phase interface is correlated with the mechanical properties. It means that the type of the interface and the parameter of γ/γ' phase are intrinsic in determining the structural and mechanical properties. Based on the geometric models and the relevant energetic calculations, we present the basic characteristic structure and the energetic states of the γ and γ' phase interface, which can be used to analyze the mechanical properties of the Ni-based single-crystal superalloys for the aircraft applications in the future.

[1] J. J. Jackson, M. J. Donachie, R. J. Henrich, and M. Gell, Metall. Trans. A **8A**, 1615 (1977).

[2] T. Khan and P. Caron, Mat. Sci. Technol. **2**, 486 (1986).

[3] G. L. Erickson, in *Superalloys 1996*, edited by R. D. Kissinger *et al.* (The Minerals, Metals and Materials Society, Warrendale, 1996), p. 35.

[4] A. F. Voter and S. P. Chen, in *High Temperature Ordered Intermetallic Alloys*, edited by R. W. Siegel *et al.*, MRS Symposia Proceedings No. 82 (Materials Research Society, Pittsburgh, 1987), p. 175.

[5] S. Lay, J. M. Missiaen, and R. Bonnet, Scr. Mater. **35**, 885 (1996).

[6] Z. P. Luo, Y. Tang, Z. Wu, M. J. Kramer, and R. W. McCallum, Mater. Charact. **43**, 293 (1999).

[7] Z. P. Luo, Z. T. Wu, and D. J. Miller, Mater. Sci. Eng., A **354**, 358 (2003).

[8] J. X. Zhang *et al.*, Metall. Mater. Trans. A **33A**, 3741 (2002).

[9] J. X. Zhang *et al.*, in *Superalloys 2004*, edited by T. E. Howson *et al.* (The Minerals, Metals and Materials Society, Warrendale, 2004), p. 189.

[10] Y. Koizumi *et al.*, in *Superalloys 2004*, edited by T. E. Howson *et al.* (The Minerals, Metals and Materials Society, Warrendale, 2004), p. 35.

[11] C. Y. Chen, R. Schäublin, and W. M. Stobbs, Mater. Sci. Eng., A **360**, 356 (2003).

[12] J. E. Angelo, N. R. Moody, and M. I. Baskes, Modell. Simul. Mater. Sci. Eng. **3**, 289 (1995).

[13] J. E. Angelo and M. I. Baskes, Interface Sci. **4**, 47 (1996).

[14] Y. Mishin, D. Farkas, M. J. Mehl, and D. A Papaconstantopoulos, Phys. Rev. B **59**, 3393 (1999).

[15] F. J. Cherne, M. I. Baskes, and P. A. Deymier, Phys. Rev. B **65**, 024209 (2001).

[16] D. Farkas, D. Roqueta, A. Vilette, and K. Ternes, Modell. Simul. Mater. Sci. Eng. **4**, 359 (1996).

[17] J. P. Hirth and J. Lothe, *Theory of Dislocations* (McGraw-Hill, New York, 1968), p. 201.

[18] L. E. Murr, *Interfacial Phenomena in Metals and Alloys* (Addison-Wesley, Reading, MA, 1975).